ENVIRONMENTAL RESEARCH
LETTERS

LETTER • OPEN ACCESS

Meta-analysis of North American Arctic and boreal aboveground biomass datasets: assessing accuracy, dynamics, and similarities

To cite this article: Wanwan Liang *et al* 2026 *Environ. Res. Lett.* **21** 054004

ENVIRONMENTAL RESEARCH
LETTERS

Check for updates

OPEN ACCESS

RECEIVED
11 November 2025

REVISED
14 February 2026

ACCEPTED FOR PUBLICATION
19 February 2026

PUBLISHED
3 March 2026

LETTER

Meta-analysis of North American Arctic and boreal aboveground biomass datasets: assessing accuracy, dynamics, and similarities

Wanwan Liang[1], Kirsten Bauck[2], Devon Maloney[3], Elizabeth Hoy[3,4], Paul Montesano[3,5], Mark J Lara[6,7], Daryl Yang[8], Jeremy Forsythe[2], Laura Duncanson[9], Xanthe Walker[2] and Jonathan A Wang[1,*]

[1] School of Biological Sciences, University of Utah, Salt Lake City, UT, United States of America
[2] Department of Biological Sciences, Center for Ecosystem Science and Society, Northern Arizona University, Flagstaff, AZ, United States of America
[3] NASA Goddard Space Flight Center, Greenbelt, MD, United States of America
[4] Global Science and Technology, Inc., Greenbelt, MD, United States of America
[5] ADNET Systems, LLC, Bethesda, MD, United States of America
[6] Department of Plant Biology, University of Illinois, Urbana, IL, United States of America
[7] Department of Geography, University of Illinois, Urbana, IL, United States of America
[8] Environmental Sciences Division, Oak Ridge National Laboratory, Oak Ridge, TN, United States of America
[9] Department of Geographical Sciences, University of Maryland, College Park, MD, United States of America
[*] Author to whom any correspondence should be addressed.

E-mail: jon.wang@utah.edu

Keywords: ABoVE, aboveground biomass map, carbon accounting, meta-analysis, disturbance, North America, Arctic boreal

Supplementary material for this article is available online

Abstract

The North American arctic and boreal regions (ABRs) are rapidly warming and experiencing intensifying disturbances. Accurately quantifying aboveground biomass (AGB) is critical for understanding the impacts of these changes on the carbon cycle and for designing climate change mitigation strategies. Several AGB maps have been developed for the North American ABRs, including recent contributions from National Aeronautics and Space Administration's Arctic-Boreal Vulnerability Experiment (ABoVE) campaign. However, these maps differ widely in training data, methodology, and resulting AGB density estimates. Presently, a comprehensive comparative evaluation is lacking, making it difficult for users to select datasets suited to their research or management needs. Here, we conducted a comparative analysis of nine AGB density datasets across North American ABRs, specifically for Alaska and Canada. We (1) summarized AGB by ecoregion and Canadian provinces, (2) evaluated their accuracy against field-based measurements, (3) analyzed spatial and temporal similarities among datasets, and (4) assessed their ability to capture disturbance (fire and harvest) impacts on AGB. We found substantial variation in regional and local AGB estimates across datasets, with overall accuracy ranging from $R^2 = 0.25$–0.62 and Bias% from -47.8% to 69.9% when validated against field plots. Despite these differences, most datasets have comparatively consistent spatial patterns in AGB ($r > 0.8$ for most cases). In contrast, agreement on the temporal patterns of AGB change is generally low. We found datasets with spatial resolutions $\leqslant 300$ m are capable of capturing disturbance impacts on AGB dynamics, though sensitivity varies across products. Our findings and dataset summary provide guidance for selecting appropriate AGB datasets for different applications within our study area. Our analysis also highlights the need to decrease map bias and increase capability to detect temporal change to decrease uncertainty of AGB datasets potentially by using training data which is representative of major plant functional types within the mapped area.

1. Introduction

Biomass is a key indicator of ecosystem structure and a central component of terrestrial carbon stock estimates, which directly influence greenhouse gas fluxes and, in turn, climate feedbacks (IPCC 2019). Quantifying aboveground biomass (AGB) stocks is thus essential to understand terrestrial carbon cycling, inform sustainable forest management, and support climate change mitigation efforts (Goetz *et al* 2009, Pan *et al* 2011). International policy frameworks, such as the United Nations' Reducing Emissions from Deforestation and Forest Degradation (REDD+), and international treaties, such as the 2015 Paris Agreement, have emphasized the need for robust carbon accounting and spatially consistent biomass estimates (UNFCCC 2015). These needs are especially urgent in high-latitude Arctic-boreal regions (ABRs), where climate warming and disturbances are rapidly increasing (Seidl *et al* 2017, Foster *et al* 2022, Rantanen *et al* 2022).

The National Aeronautics and Space Administration's (NASA) Arctic-Boreal Vulnerability Experiment (ABoVE) supported a decade-long field campaign to study the rapidly changing ecosystems of high-latitude North America (Miller *et al* 2019). Throughout the campaign, researchers integrated data from field and airborne platforms with spaceborne remote sensing technologies to develop a series of AGB products for the ABRs from landscape to biome scales (Wang *et al* 2021, Kraatz *et al* 2022, Duncanson *et al* 2023, Liang *et al* 2025, Orndahl *et al* 2025). These datasets, with spatial resolution ranging from 30 to 100 m, provide the scientific community with an unprecedented view of biomass distribution, dynamics, and associated uncertainties across the ABRs of North America.

In addition to the AGB datasets developed through the ABoVE campaign, researchers worldwide have developed multiple AGB datasets for the North American ABRs at the regional-scale with 30 m resolution (Matasci *et al* 2018, Guindon *et al* 2023) and at the global-scale with medium to coarse-resolution (Liu *et al* 2015, Hu *et al* 2016, Spawn and Gibbs 2020, Harris *et al* 2021, Santoro *et al* 2021, Xu *et al* 2021, Yang *et al* 2023). Collectively, these efforts have substantially expanded the spatial and temporal coverage of AGB products for ABRs.

However, despite the development of various datasets, AGB estimates in ABRs from satellite data remain highly uncertain. Persistent challenges include field data availability, scaling mismatches between field and remote sensing data, and short growing seasons that curtail satellite data availability at high-latitudes (Metcalfe *et al* 2018, Gabarró *et al* 2023). Moreover, high-latitude forests are subject to dynamic and spatially heterogeneous disturbance regimes (e.g. fire, timber harvest), which further complicate AGB estimation. These challenges increase the uncertainty of AGB estimates in high latitude and may make certain characteristics of datasets more appealing to potential users, e.g. sensitivity to disturbances. However, there still lacks a consensus or systematic evaluation that addresses the accuracy, spatial and temporal consistency, and sensitivity of different datasets to disturbance across the North American ABRs. This makes it difficult for researchers, managers, and policymakers to identify the datasets most appropriate for their specific applications.

To address the absence of a comprehensive evaluation of AGB products in the North American ABRs, we present a meta-analysis of nine remote sensing based datasets. Specifically, we (1) summarized the methodologies used for mapping AGB, (2) quantified AGB density by ecoregion and jurisdiction, (3) evaluated map accuracy, (4) analyzed the similarity of estimated AGB density across space and, when possible, through time, (5) evaluated the sensitivity of AGB responses to disturbance, and (6) lastly we summarized the products that are suitable for different applications. Conducted at the conclusion of NASA's ABoVE campaign, this analysis aims to summarize the characteristics of existing datasets produced through ABoVE and other programs within North American ABRs, specifically for Alaska and Canada, identify their strengths and recommended applications for user communities engaged in carbon monitoring or accounting for North American ABRs, and inform future biomass mapping initiatives.

2. Methods

2.1. Study area and datasets included

We limited our study to Alaska and Canada to focus on the ABoVE domain and North America ABRs (figure 1). Our study area includes tundra, boreal, and temperate biomes, but we generally refer to our study area as tundra, boreal, or ABRs for conciseness, as 81% of the study domain falls within these two biomes (Olson *et al* 2001). We focused on datasets that are publicly available, which cover a regional or larger spatial scale for 2010 or more recent years with spatial resolution no coarser than 10 km. Consequently, we included nine datasets with a range of study periods, temporal and spatial coverage, and model calibration approach (table 1). Note that this collection of datasets is not exhaustive, though it represents what we believe most of the recent major releases relevant to North American ABRs.

Among the nine datasets, three have global extents, two cover specific biomes, and four are regional or continental (table 1). AGB pools mapped include live woody, total woody (live and dead), and total live biomass (woody and non-woody), with

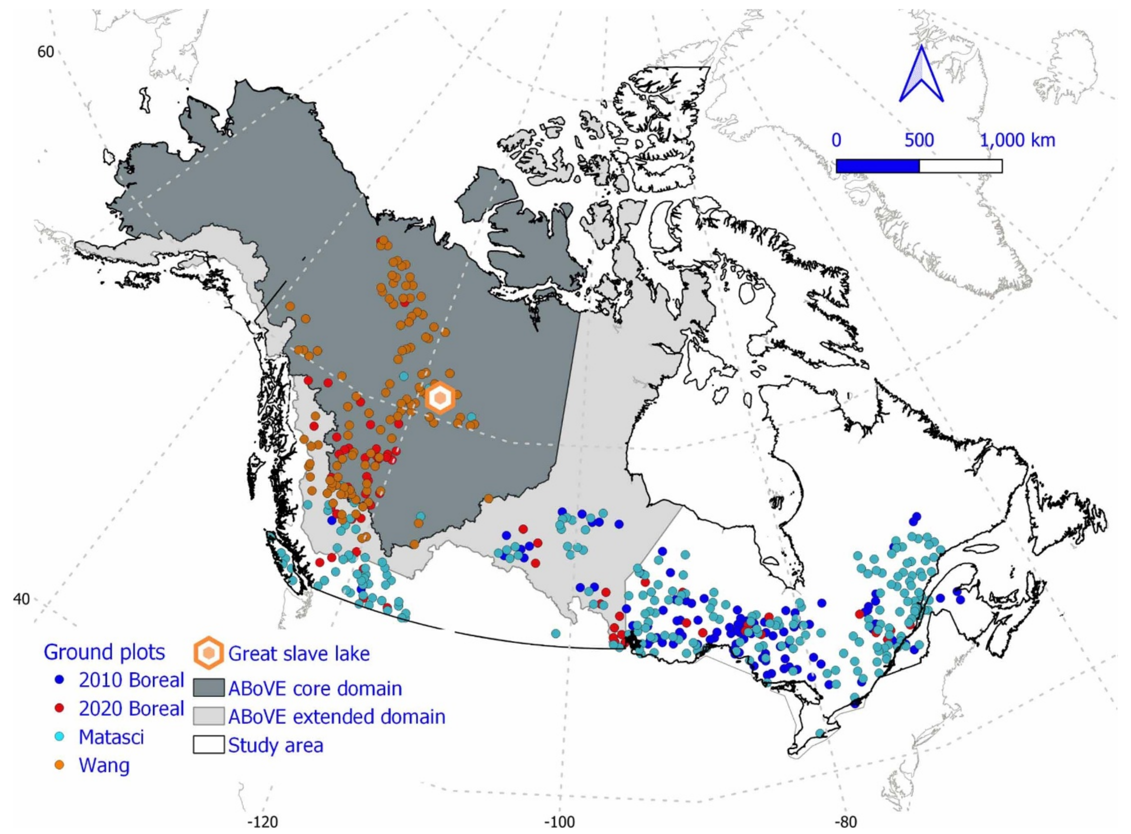

Figure 1. Study area and distribution of ground plots used for map evaluation ($n = 598$). Definition of 2010 Boreal and 2020 Boreal is described in section 2.4.

woody AGB most common (table S1). Five datasets provide a single-year AGB map and four include multiple years, at resolutions ranging between 30 m and 10 km. Training data most often came from space-borne lidar (e.g. ICESat-2), ground plots, or airborne Lidar. Landsat is the primary source of predictors and is used by all non-global datasets. More detailed descriptions of dataset creation methods are in the supplementary materials section 1. To efficiently reference each dataset, we used the first author's last name, except for the European Space Agency Climate Change Initiative (ESA CCI) data, which we refer to as ESA CCI 2010 or ESA CCI 2020 based on the year of map analyzed. Table S2 summarized the analysis we conducted for each dataset.

2.2. AGB density comparison and visualization

To analyze spatial variation of mapped AGB among datasets, we derived the mean AGB by level II ecoregions from EPA (U.S. Environmental Protection Agency 2010) (figure S1) and Level 1 administrative units of Canada (Government of Canada 2019). All datasets were resampled to 30 m and were projected to an equal area projection (ESRI:102001) for comparison. We also generated common masks for tundra and boreal regions separately by identifying overlapping spatial extents across datasets to ensure the same areas were included across datasets for fair comparison (figure S2). We then calculated mean AGB for each dataset for the masked region selected based on the dataset's spatial extent. For multi-year datasets, we selected the most recent mapped year for Wang (i.e. 2014) and Xu (i.e. 2019), and used the 2020 map for ESA CCI and Liang.

To visualize detailed differences among datasets, we showed the mapped AGB at a landscape scale in the Great Slave Lake (GSL). GSL has a wide range of AGB (0–140 Mg ha^{-1}), and is a key region for numerous ecosystem vulnerability and resiliency studies (Kraatz *et al* 2022).

2.3. Accuracy evaluation with ground plots

Due to the limited number of ground plots that overlap temporally with tundra AGB maps and are independent from training data used by Liang and Orndahl datasets (Berner *et al* 2024) (table S1), the accuracy evaluation is only conducted for the boreal region by using reference AGB from ground plots from the Multi-Agency Ground Plot (MAGPlot) program of Canada (MAGPlot 2024). Most plots are circular with a diameter of 22 m (equivalent to 0.04 ha). We therefore excluded Xu dataset for this evaluation due to its coarse spatial resolution (10 km) (table S2). The Liang dataset was trained using the majority of these plots (personal communication), so we only included plots that were at least 1 km away from their training data for this evaluation.

Table 1. Summary of nine aboveground biomass (AGB) density datasets.

Dataset	Resolution, timespan	Domain	AGB pool	Training data	Source of primary predictors	Model[a]	Uncertainty map
			ABoVE Datasets				
Duncanson *et al* (2023)	30 m, 2020	Circumpolar boreal biome	Total woody	ICESat-2 Lidar plots	Harmonized Landsat Sentinel-2	DT; regional	Yes
Liang *et al* (2025)	30 m, 1984–2022	Alaska and Canada	Total woody (boreal), live total (tundra)	Ground plots, airborne Lidar, UAS	Synthetic Landsat	DT; ecoregion	
Orndahl *et al* (2025)	30 m, 2020	Circumpolar tundra biome	Live total and live woody	Ground plots		DT; global	
Wang *et al* (2021)	30 m, 1984–2014	ABoVE core domain	Live woody	ICESat Lidar plots			
			Canadian Forest Service Datasets				
Guindon *et al* (2023)	30 m, 2020	Canada non-tundra region	Woody	Photo plots	Landsat and Synthetic Landsat	kNN-RF; regional	No
Matasci *et al* (2018)	30 m, 2015	Canada forested ecosystems		Airborne Lidar plots	Landsat composites	kNN-RF; global	
			Global Datasets				
ESA CCI (Santoro and Cartus 2025)	100 m, 2007, 2010, 2015–2022	Global	Live woody	ICESat, ICESat2, and GEDI plots	SAR from Sentinel, ALOS PALSAR, Envisat ASAR	NLR; administrative or ecological unit	Yes
Spawn and Gibbs (2020)	300 m, 2010		Live total	Multiple biomass maps and models, land cover map, and tree cover percentage		EMM	
Xu *et al* (2021)	10 km, 2000–2019		Live woody	Ground plots, airborne Lidar, ICESat, and ALOS PALSAR	MODIS, Radar from QuikSCAT	DT; global	No

UAS: unoccupied aerial systems.

[a] Models are bucketed as decision tree (DT) family model, k-nearest neighbors-random forest (kNN-RF), non-linear regression (NLR), or ensemble of multiple maps/models (EMMs); and are categorized by which scale or unit the model was calibrated. 'Global' means a single model was calibrated for the mapped area.

For time-series maps, we used ground plots surveyed in the same years as the mapped years. For non-time-series maps, we used plots surveyed within one year of the mapped year. We used live and total woody AGB from ground plots to evaluate datasets representing live and total woody AGB, respectively. As most ground plots lacked non-woody AGB measurements, we applied ecoregion and land cover (Hu *et al* 2025) specific correction factors (table S3) derived from AGB estimates of different pools from the Canadian National Forest Inventory plots (NFI Canada 2021) (supplementary figure S3), to convert live woody AGB to live total AGB for evaluating the Spawn dataset.

Because of the various timeframes described above, we categorized datasets into two major groups: (1) 2010 Boreal including datasets from ESA CCI 2010, Spawn, and Liang, and (2) 2020 Boreal including datasets from Duncanson, Guindon, Liang, and ESA CCI 2020. The same ground plots were used to evaluate datasets within each group (figure 1).

2.4. Dataset similarity analysis

To evaluate spatial and temporal similarity among datasets, we conducted two evaluations using Pearson correlation and % difference as evaluation metrics. The first evaluation examined similarity of spatial patterns and was conducted for boreal and tundra regions separately. We randomly sampled 800 and 350 circular polygons across boreal and tundra regions, respectively, and derived the mean AGB per polygon to compare their similarity. To reconcile the scale differences across datasets, i.e. 30 m–10 km, we used a radius of 10 km for the circular polygon (i.e. area $\sim$300 km^2).

The second evaluation was focused on the similarity of the temporal pattern and was conducted for time-series datasets and the boreal region using the same polygons as described above. Due to differences in spatial and temporal coverage of datasets, we derived the AGB change between 2010 and 2000 maps from Liang, Wang, and Xu for ABoVE core domain, and the AGB change between 2019 and 2010 maps from ESA CCI, Liang, and Xu for the Canada domain.

2.5. Evaluation of sensitivity to harvest and fire disturbances

We used ground plots with harvest disturbance predating the field measurement to evaluate the sensitivity of different datasets to harvest. We used ground plots surveyed in the same years as the mapped years and within two years of the mapped year for time-series and non time-series maps, respectively. Xu and Wang datasets were excluded due to their coarse spatial resolution and insufficient plots, respectively (table S2). Similar to accuracy assessment, the same plots were used for the same dataset groups.

To evaluate how different datasets capture the impact of fire on AGB dynamics, we used fire perimeter polygons from the National Burned Area Composite of Canada (Natural Resource Canada 2024). Considering heterogeneity within the study area may lead to potential difference of post-fire recovery pattern, we conducted this evaluation by each of the three biggest ecoregions (figure S4) based on EPA Ecoregion Level 1 (U.S. Environmental Protection Agency 2010): the Northwestern Forested Mountains (NWFMs), Northern Forests (NFs), and Taiga.

Different approaches were applied for time series datasets with 2 or more decades of temporal coverage (Group 1), including Liang, Xu, and Wang, and other datasets covering boreal region (Group 2) (figure 2). For Group 1, we used fire polygons disturbed in 1985–1987 to evaluate Liang and Wang datasets, and those disturbed in 2001–2003 to evaluate Xu dataset. For each fire polygon, we tracked AGB predictions from one year before disturbances to the latest mapped year, assessing each dataset's ability to capture fire-related AGB loss and post-fire recovery. For Group 2, we used the space-for-time approach. We selected fire polygons disturbed between 1985 and one year before the mapped year and derived predicted AGB. To estimate AGB loss from wildfire, we created a paired control polygon (PCP), i.e. a 1 km buffer around each fire polygon that was not significantly affected by fire. The mean AGB difference between PCP and fire polygon was used as an approximation of fire-caused AGB loss. Additional details on fire polygon selection are in supplementary 2.1. Given their similar temporal and spatial coverage, the Duncanson and Guindon datasets were evaluated using the same fire polygons. Similarly, a same set of fire polygons were used to evaluate ESA CCI 2010 and Spawn datasets.

3. Results

3.1. AGB density comparative summary and visualization

Among datasets covering all tundra regions of North America (figures 3 and S5), Liang, Orndahl, and Spawn had similar AGB in the Northern Arctic ($\sim$1 Mg ha^{-1}), higher than that from ESA CCI ($\sim$0 Mg ha^{-1}) and significantly lower than that from Xu ($\sim$9 Mg ha^{-1}). For the Southern Arctic, ESA CCI also estimated the lowest mean AGB ($\sim$1 Mg ha^{-1}) compared to the other four maps ($\sim$4–5 Mg ha^{-1}).

For datasets covering boreal regions, the majority captured similar coarse AGB spatial patterns (figure 3), i.e. highest in the southwestern region and lowest in the northernmost region. However, the mean AGB density varied significantly among datasets. For non-tundra regions of Canadian provinces (figures S6 and S7), the ESA CCI dataset had the highest AGB across the area (55.79 $\pm$ 69.87 Mg ha^{-1}; mean and standard deviation), followed by Liang (48.96 $\pm$ 63.24 Mg ha^{-1}),

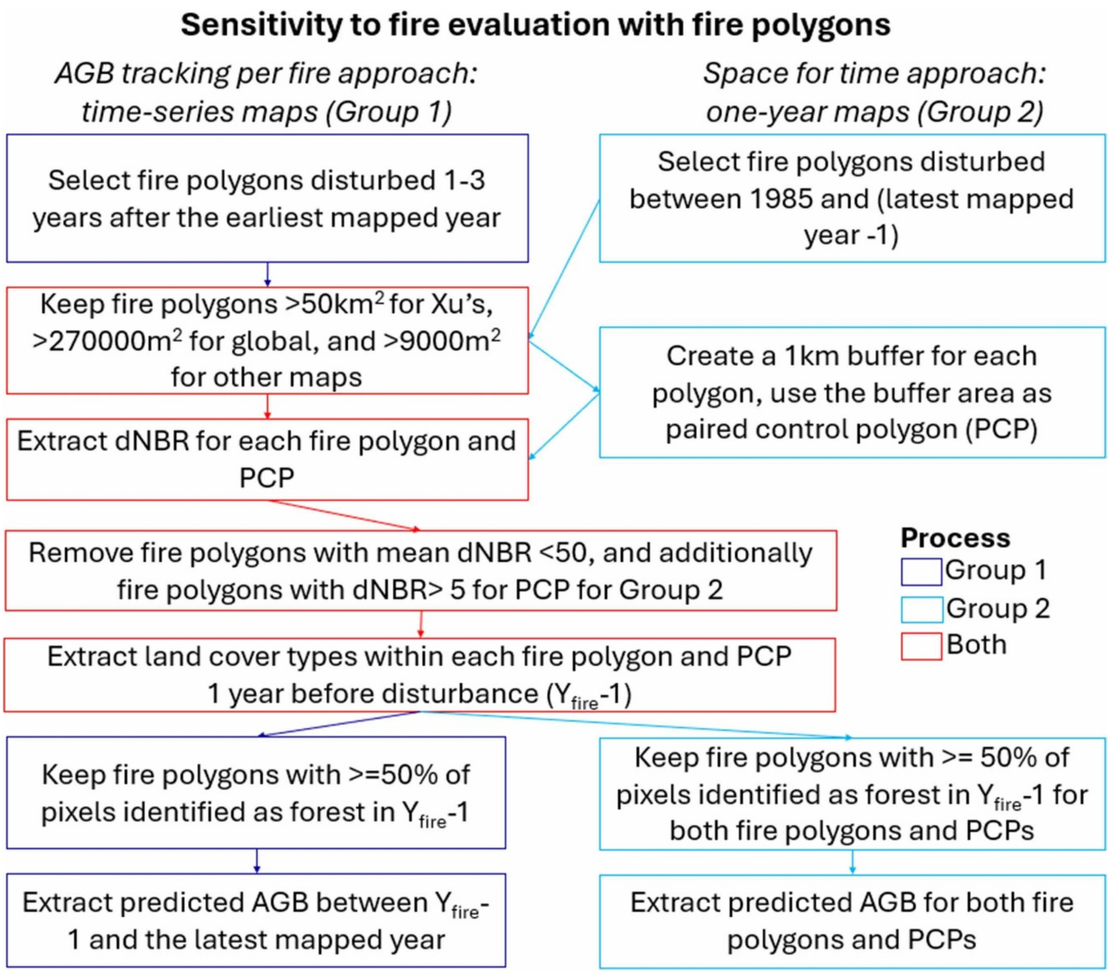

Figure 2. Workflow for sensitivity evaluation of datasets to fire disturbance using fire perimeter polygons, i.e. fire polygons.

Spawn (46.06 ± 52.71 Mg ha^{-1}), Guindon (43.79 ± 58.68 Mg ha^{-1}), Matasci (38.94 ± 65.78), Xu (31.94 ± 25.67 Mg ha^{-1}), and Duncanson (30.26 ± 38.98 Mg ha^{-1}). This ranking of predicted AGB density by datasets at regional scale is consistent with the AGB estimates at local scale in the GSL region (figures 4 and S8), where the stand-level differences among datasets could be visually seen. Most datasets predicted higher AGB estimates in densely vegetated areas. However, due to the coarse resolution, local-scale patterns in AGB were not clear in the Xu dataset (figure 4).

3.2. Accuracy evaluation for boreal region

Accuracy varied widely among datasets (figure 5). Within the 2020 dataset group (figures 5(a)–(d)), Liang performed best with the highest R^2 (0.52) and lowest bias (−4.1%). Duncanson had a high R^2 (0.42) but also a high bias (−47.8%), while ESA CCI had a relatively low R^2 (0.25) and a high bias (69.9%). Guindon showed moderate accuracy (R^2 = 0.36, bias = −17.5%). Among the 2010 boreal datasets (figures 5(e)–(j)), Liang showed the highest accuracy (R^2 = 0.62, bias = −14.3%). Between the two global datasets, ESA CCI had the similar R^2 (0.41) as Spawn (0.42) but a much higher bias (32.2% vs. −15.5%). The Matasci dataset showed low R^2 (0.26) and bias (−16.6%), where many plots were predicted 0 due to the use of a land cover map to assign 0 to non-forest pixels. Lastly, the Wang dataset had a high R^2 (0.46) and a bias of −25.9%.

3.3. Similarity analysis

3.3.1. Tundra region

When aggregated to a common ∼300 km^2 scale, maps covering the tundra region showed strong correlations ($r > 0.75$) among Liang, Orndahl, and Spawn datasets, with mean AGB densities of 1.9–2.2 Mg ha^{-1} mapped by all three datasets (figure 6(a)). In contrast, ESA CCI 2020 correlated strongly only with Liang (r = 0.83) and estimated a mean density of 1.1 Mg ha^{-1}. The Xu dataset showed weak-to-moderate correlations with others (r = 0.12–0.37) and reported a mean AGB density of 5.5 Mg ha^{-1}, i.e. several times higher than other datasets.

3.3.2. Boreal region

For the boreal region, AGB estimates were highly correlated ($r > 0.7$) among all datasets, except for Xu and Wang (r = 0.67) (figure 6(b)). Excluding the

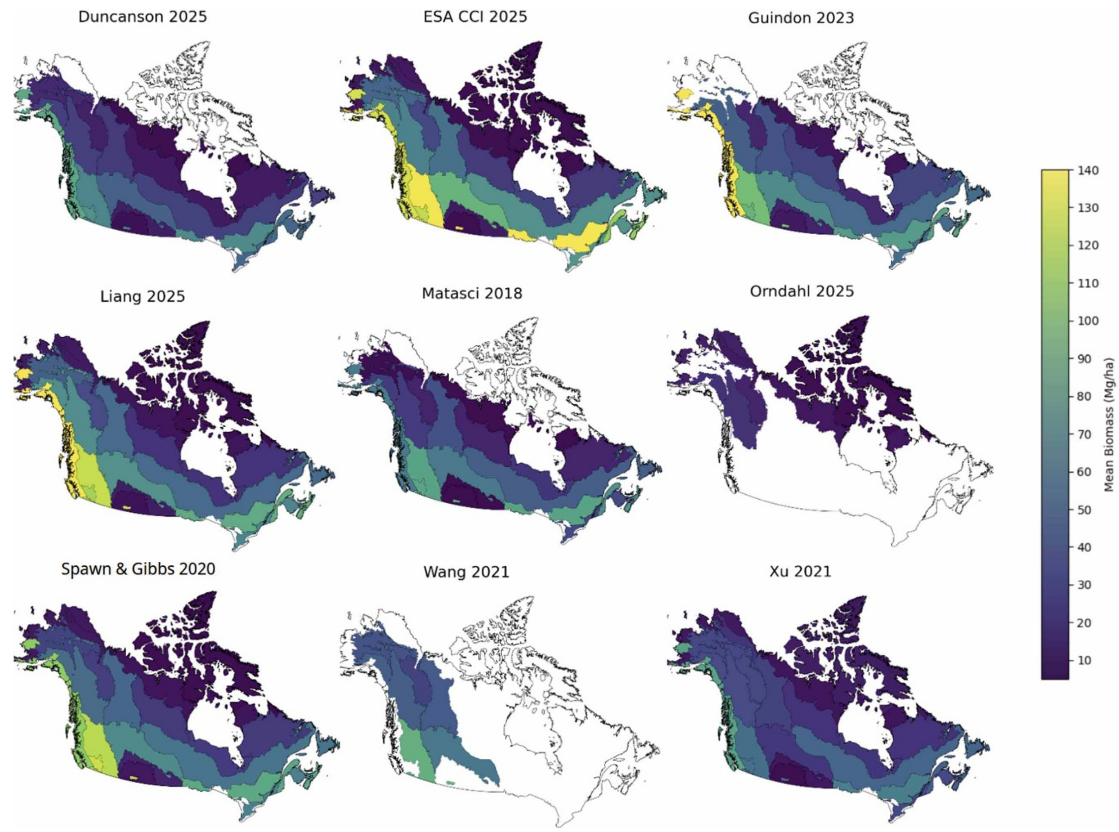

Figure 3. Mean AGB density (Mg ha^{-1}) by dataset (and dataset publication year) across EPA Level II ecoregions (figure S1). Figure S5 presents mean values by ecoregion.

Xu dataset, the correlation between any two dataset was at least 0.83, indicating that most maps capture similar broad spatial patterns of AGB density despite the significant variability in the absolute value (figures 6(b), S6 and S7).

However, the correlation of AGB temporal changes among datasets was mostly weak to moderate (r: −0.12–0.36) (figure S9). High correlation was only observed between Liang and Wang ($r = 0.74$) (figure S9(a)). The Liang and Wang datasets also had high agreement on the AGB change sign (86.8%), while agreement on change sign was generally low (<65%) among other datasets (figure S9).

3.4. Evaluation of capability to capture disturbance-caused AGB dynamics

3.4.1. Harvest disturbance

All evaluated datasets captured some degree of recovery (figure 7). Among the 2020 boreal maps, Liang and Guindon datasets correlated most strongly with reference AGB ($r = 0.57$–0.64; table S4), but both datasets showed overprediction of AGB (Bias% > 35%). The Duncanson dataset also captured the recovery dynamics well ($r = 0.47$) with much lower bias (5.1%, table S4). Matasci map captured the overall recovery pattern ($r = 0.55$, Bias% = −1.7%, table S4), but with considerable noise in the first period. Despite coarser resolution, global datasets ESA CCI (100 m) and Spawn (300 m) also showed gradual recovery (figure 7). However, both ESA CCI (Bias% ≈ 200%, table S4) and Spawn & Gibbs (156.2%, table S4) severely overestimated AGB.

3.4.2. Fire disturbance

All datasets showed sensitivity to fire (i.e. losing substantial biomass following fire and slow post-fire recovery), with the exception of the Xu dataset. Therefore the Xu dataset was excluded from further summarization in this section. All datasets showed a U-shaped post-fire recovery curve in two or all ecoregions, which might be explained by two processes: (1) faster decomposition of dead AGB than regrowth of live AGB right after fire (Seedre *et al* 2014) and (2) continued postfire tree mortality after fire (Busby *et al* 2024).

The time-series datasets from Liang and Wang both showed the typical U-shape pattern across all ecoregions, with Liang consistently estimating higher AGB than Wang (figure 8(a)). Duncanson and Guindon showed similar post-fire recovery in NWFM and Taiga (figure 8(b)), while in NF Duncanson also showed a U-shape while Guindon showed more of a monotonic increase. Guindon indicated a much

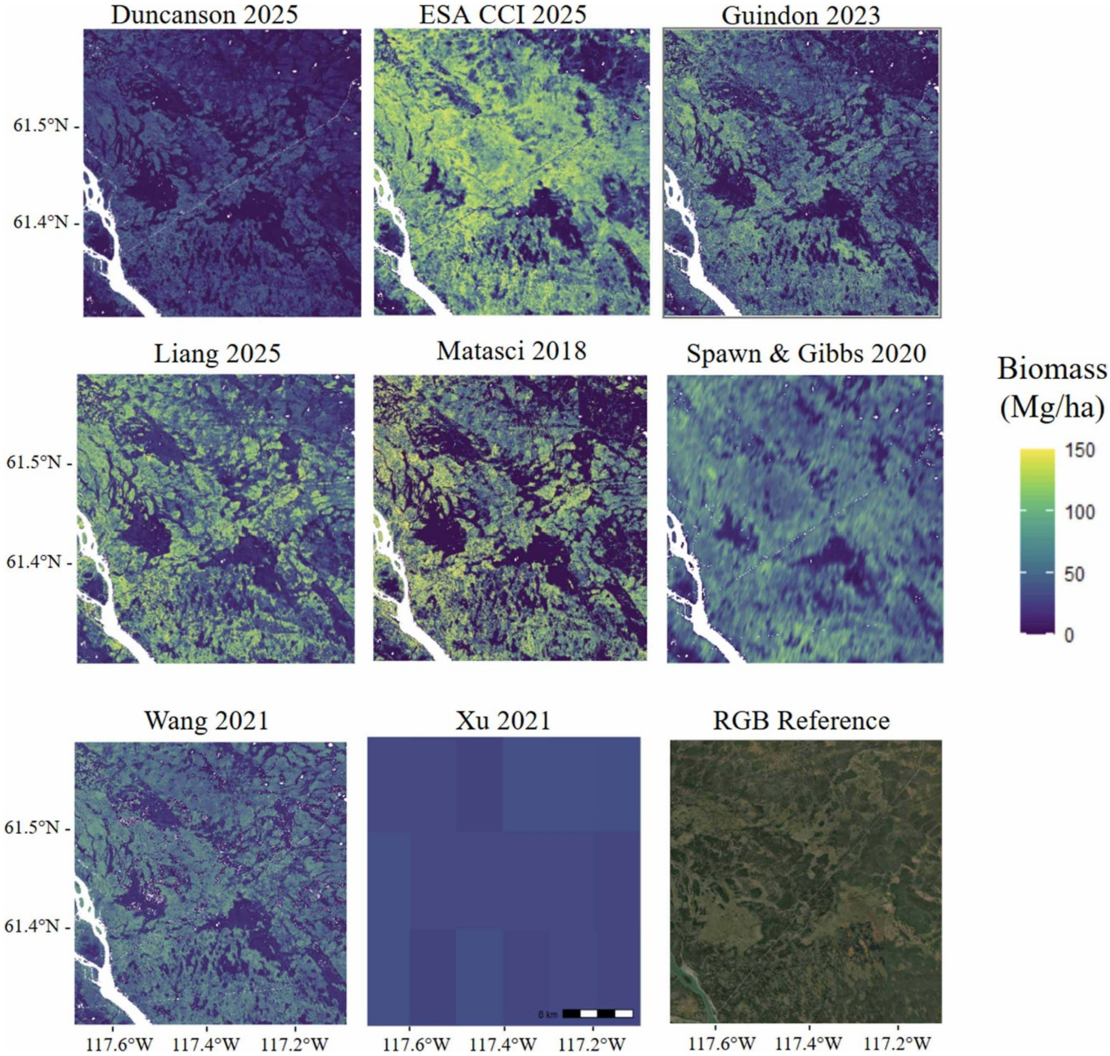

Figure 4. Comparison of mean AGB estimates (Mg ha^{-1}) across datasets for the Great Slave Lake. RGB reference from the ESRI satellite imagery basemap. Darker areas depict forest cover, while lighter areas depict wetlands and herbaceous cover. RGB is short for red, green, and blue.

higher recovery rate 26–30 years post-fire compared to both earlier periods in its own map and other datasets, which may not be realistic. ESA CCI (Santoro and Cartus 2025) and Spawn (Spawn and Gibbs 2020) showed similar recovery in NWFM and NF but differ in magnitude (figure 8(b)). However, Spawn showed much smaller AGB loss during 1–5 years post-fire than all other datasets, suggesting possible overestimation of AGB during that period. The Matasci dataset showed a clear U-shape in NF, but weakly in Taiga and not in NWFM (figure 8(b)).

4. Discussion

4.1. Dataset summary

For datasets covering tundra regions, the estimated AGB patterns and density are similar among Liang, Orndahl, and Spawn, while ESA CCI predicted lower AGB density and Xu predicted much higher AGB density. For boreal regions, datasets from Duncanson, ESA CCI 2010, Liang, Spawn, and Wang well-represented the spatial patterns of AGB, evidenced by the relatively high R^2 (0.41–0.69) between reference and predicted AGB (figure 5). Datasets generally predicted similar spatial patterns of AGB when upscaled to $\sim$300 km^2 scale (figure 6, $r > 0.8$ for most cases). However, they differed significantly in absolute AGB density. Based on the magnitude of mean AGB density (figures 3, S6 and S7), datasets can be ranked from high to low in the following order: ESA CCI, Liang, Spawn, Guindon, Matasci, Wang, Xu, and Duncanson.

The percent uncertainty of AGB estimates among datasets (figure 9), calculated as the ratio of standard deviation to mean of AGB estimates from different AGB datasets (details in table S1), is high in tundra regions (i.e. 23.6%–130.3%) due to the low AGB density. For non-tundra regions and excluding the agriculture intensive regions in Prairies (figure S1), percent uncertainty varied between 20.6% and 53.3%

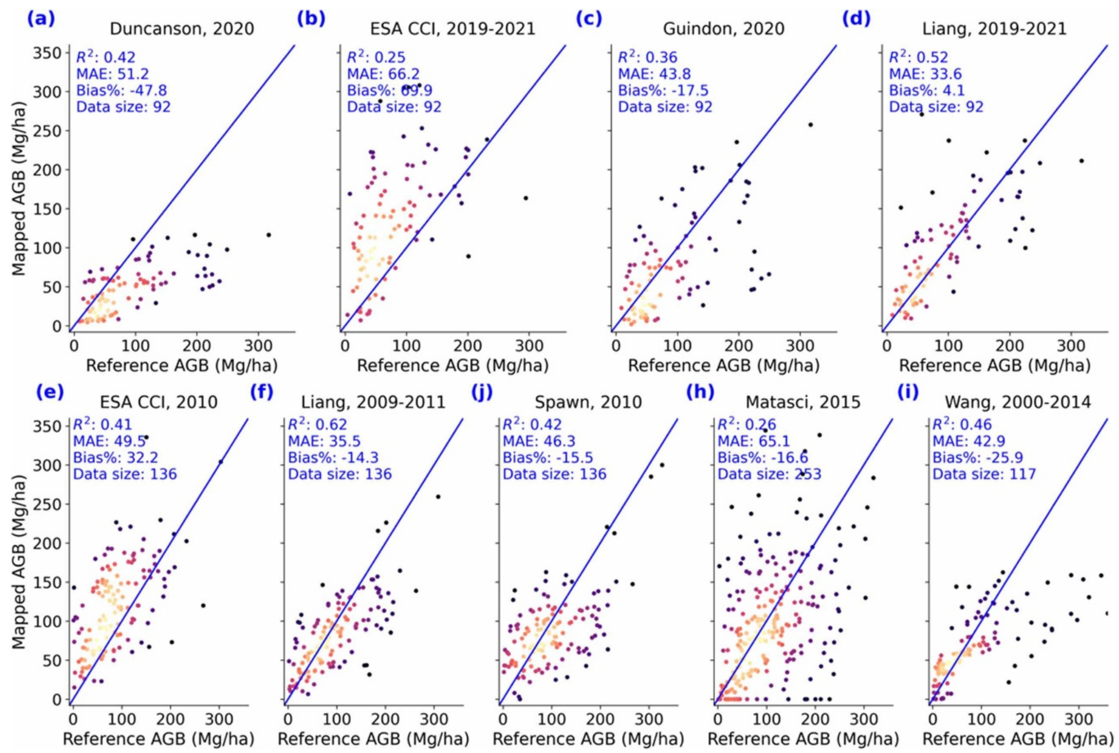

Figure 5. Mapped aboveground biomass (AGB) versus reference AGB for each dataset, and year of map used. The same validation data were used for 2020 boreal maps in (a)–(d) (top row), and the same data were used for 2010 boreal maps in (e)–(j) (bottom row). Blue lines indicate 1:1 lines, and the color scale from bright to black represents data density from high to low. MAE: mean absolute error.

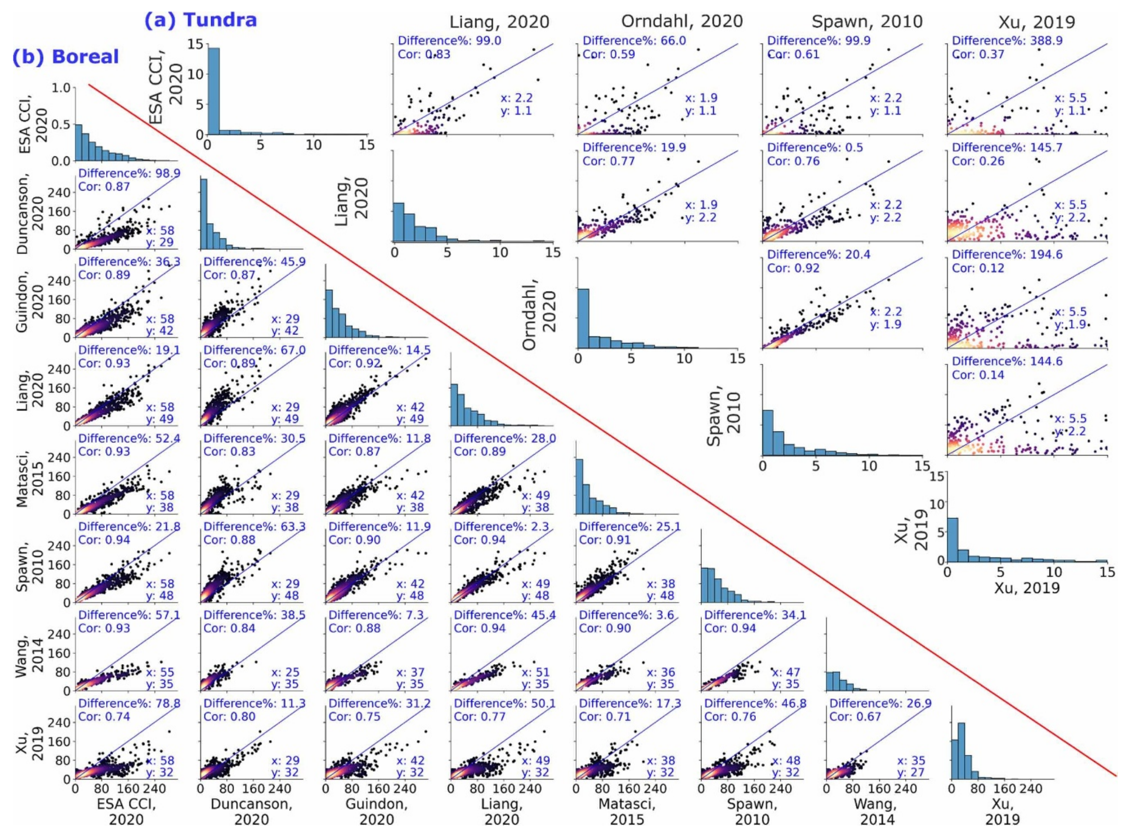

Figure 6. Similarity analysis among datasets, year of map covering the (a) entire Tundra region of North America and (b) boreal region of study area. *x* and *y* in subplots represent means of *x* and *y* axis, respectively. For plot (b), all comparisons use the same polygons from Canada, except the ones with Wang, which use polygons from the overlapping areas between Canada and ABoVE core domain.

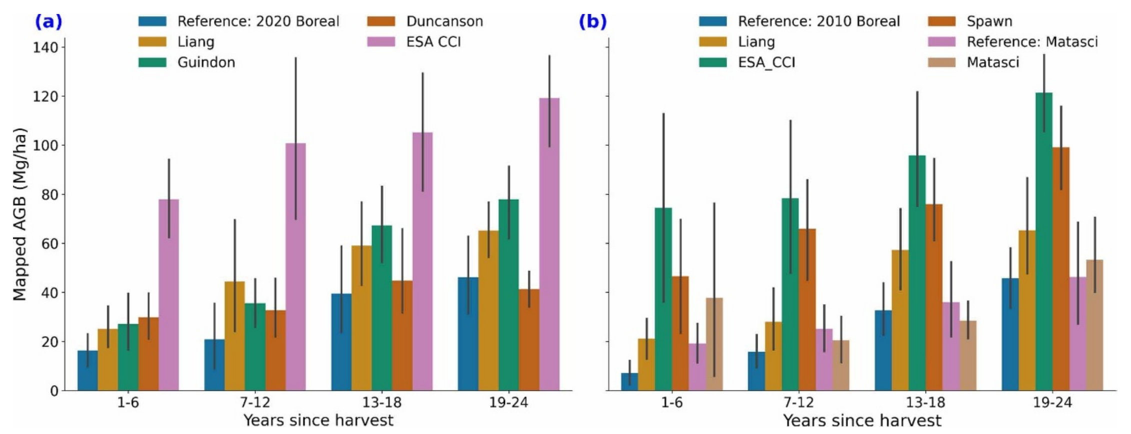

Figure 7. Mean and 95% confidence interval of reference and mapped AGB for harvested plots from (a) 2020 Boreal dataset group and (b) 2010 Boreal group + Matasci map for 2015. Within each group, datasets are ordered by correlation with reference AGB; bars closer to the reference indicate higher correlation (table S4).

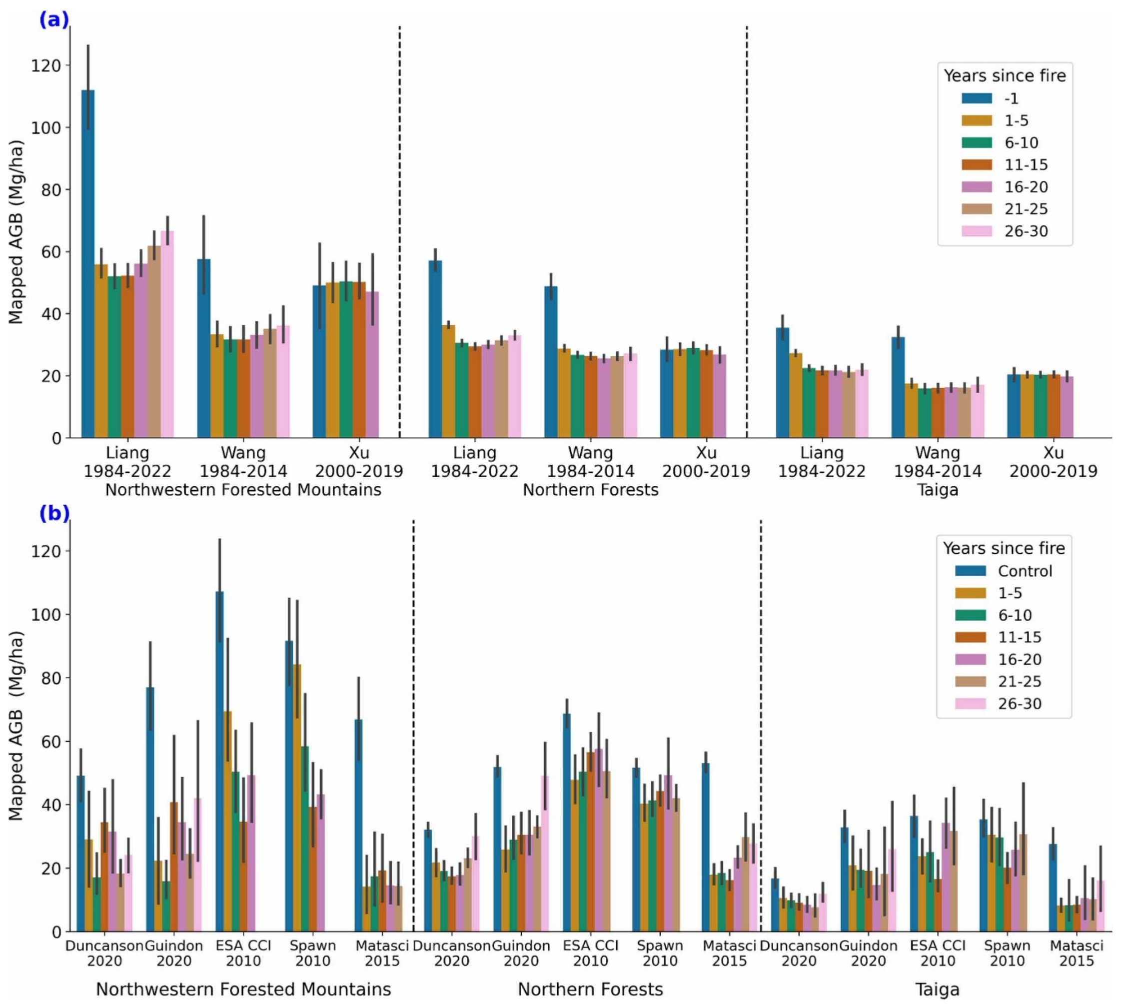

Figure 8. Mapped aboveground biomass (AGB) density for fire disturbance area from each dataset, mapped year, and ecoregion for (a) time-series datasets and (b) single-year datasets using a space-for-time approach. The black bar indicates the standard error of the mean mapped AGB per period. −1 means 1 year before fire, control: unburned control.

(figure 9). Within these regions, the percent uncertainty is highest in Alaska boreal interior (i.e. 53.3%) compared to other regions (i.e. 20%–34%), suggesting extra effort might be needed for this region to decrease uncertainty.

All included datasets with spatial resolution ⩽300 m and covering the boreal region can capture fire or harvest caused AGB dynamics, although with different sensitivity (figures 7 and 8). Datasets generally overestimate AGB density in areas affected

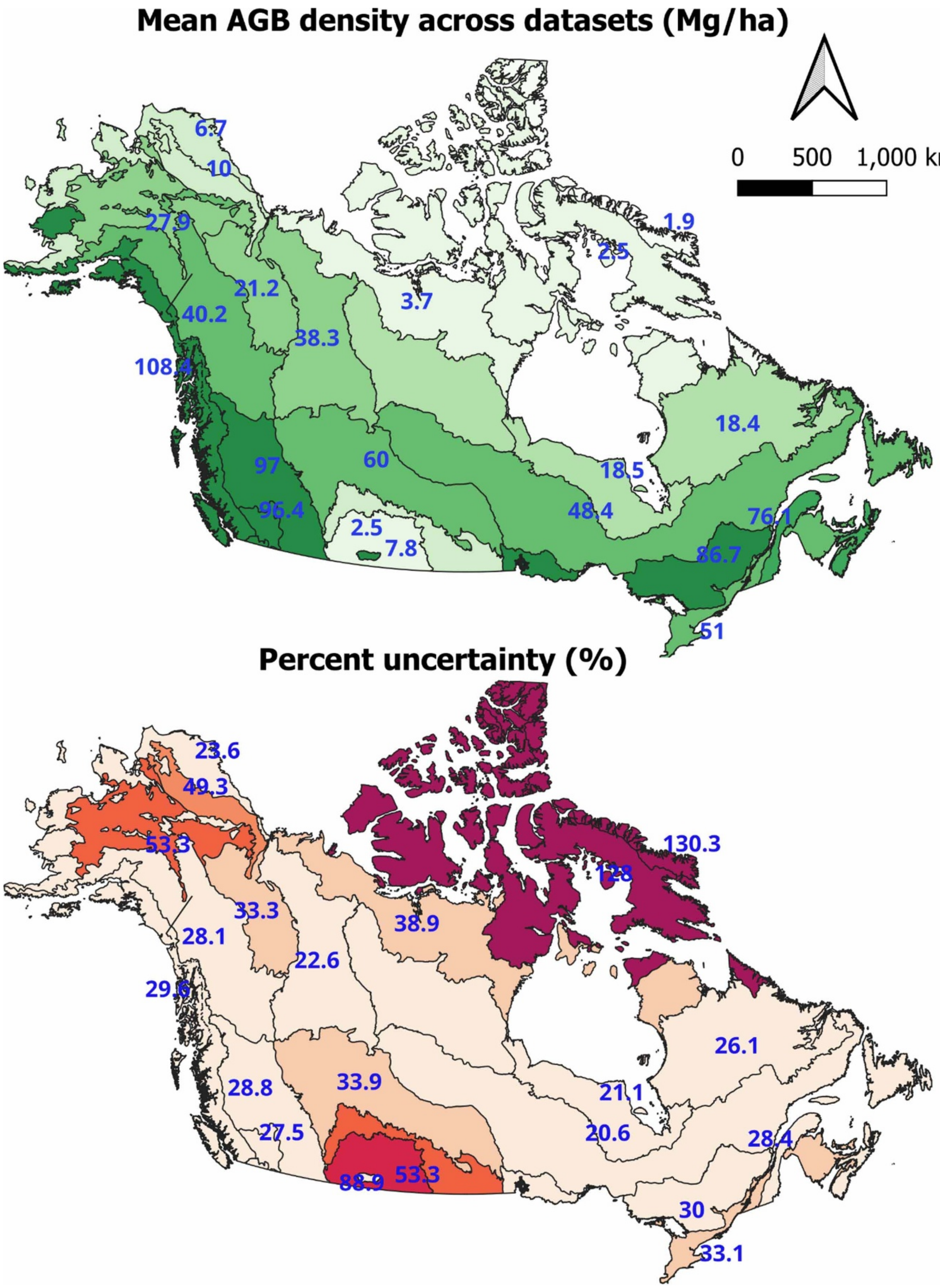

Figure 9. Mean AGB density from different datasets and percent uncertainty (calculated as the ratio of standard deviation of AGB estimates to mean of AGB estimates) by ecoregion level II.

by timber harvest 2–3 decades ago (figure 7), with Duncanson showing the lowest bias (5.1%) and ESA CCI 2020 the highest (178.9%). However, the similarity of temporal AGB change patterns at decadal scale were generally low across time-series datasets (figure S9). The high variability in AGB density estimates and low agreement on temporal trends suggest that careful dataset selection and weighting might be needed for readers interested in deriving ensemble products. Understanding the appropriate applications of each dataset, as discussed in section 4.2, could help guide this process.

We emphasize that our evaluations are focused on the ABRs of North America, and resulting findings may not apply to the spatial domain outside of our study area. For example, ESA CCI biomass maps are produced globally and may not exhibit overestimations in other domains (ESA CCI Biomass 2024).

Similarly, the Duncanson map is pan-boreal, and the underestimations here are not apparent in Eurasia where there is no country-level bias detected. The product's underestimation of total Canadian AGB of 30% is a relative outlier compared to other northern country estimates, which is mainly caused by limited field plots used as training data from Canada (more details in Duncanson *et al* 2025). Including more Canadian data to decrease bias is noted as a key target for future updates.

4.2. Suitability for North American ABRs application

For user communities working with AGB products in the North American ABRs, it is essential to select datasets aligned with their specific research or management goals. We present recommendations for four primary application areas pertinent to the ABRs.

Estimating AGB stocks: Maps with low bias can provide AGB stock estimation without significant overestimation or underestimation. Maps that characterize uncertainty can be used to propagate uncertainty to stock totals. For boreal regions, the Liang dataset has the lowest bias followed by the Spawn and Guindon datasets. For the tundra region, the Liang, Orndahl, and Spawn datasets all give similar stock estimates on total live AGB as suggested by similar mean AGB density estimates (figure 6(a)).

Examining spatial patterns of AGB at fine scales: For analyzing AGB patterns at small spatial units (e.g. fields or landscapes), relatively high-resolution datasets that show high R^2 (e.g. $R^2 \geqslant 0.4$) with reference AGB can be preferred, which include Duncanson, ESA CCI 2010, Liang, Spawn, and Wang datasets. These datasets can be useful for evaluating AGB variation across ecotones or other complex landscapes.

Quantifying the impact of disturbances on AGB: Most datasets detect fire disturbance, estimates of fire-driven carbon loss and recovery rates vary widely (figure 8), reflecting substantial uncertainty, particularly given limited ground-based reference data. Datasets with relatively high-resolution (<100 m) are important for precisely overlapping AGB change with disturbance occurrences, as disturbances are spatially heterogeneous or occur in small patches. Time series maps from Liang and Wang provide annual AGB maps for more than 30 years thus have advantages as one can directly derive AGB loss and recovery over time. Nevertheless, using the space-for-time method, other AGB datasets can provide valuable insights on disturbance-caused AGB loss and recovery. For harvest disturbance, the Guindon and Liang datasets better capture the AGB recovery trend ($r \geqslant 0.57$, table S4) but with high overestimation (>35%), while the Duncanson dataset captured the AGB recovery dynamics with a much lower bias (~5%). ESA CCI can capture AGB recovery after harvest, but the estimated AGB could be 1.5–2 times higher than ground truth. Users may want to avoid Matasci dataset as their map only has valid predictions for forest pixels, thus may not capture early stage recovery where once forested pixels appear non-forested.

Quantifying the sensitivity of AGB dynamics to interannual weather variability: An important use of these datasets is characterizing how large-scale weather variability (e.g. heat waves or drought) impact AGB change over time and over large regional scales. In this sense, time series datasets from which annual changes in AGB stocks can be estimated over time are preferred, even when they may be spatially coarse. However, finer scale datasets can be used to identify and exclude areas experiencing disturbance thus isolating the impact of weather variability.

4.3. Similarity in spatial pattern but divergence in AGB density and temporal pattern

The majority of the boreal datasets find similar spatial patterns of AGB density ($r > 0.8$ for most cases) when upscaled to ~300 km^2 scale (figure 6(b)), suggesting datasets are spatially consistent in identifying areas of relatively low and high AGB. However, the absolute AGB density varies significantly among datasets, resulting in a significant variation of bias compared to ground-based AGB, which further adds uncertainty in carbon accounting and ESM benchmarking. For example, the AGB density from ESA CCI is nearly twice that estimated by Duncanson and Xu (figures 6(b), S6 and S7). We found global or pan-boreal datasets are generally good at capturing spatial patterns of AGB (3 out of 4 cases), evidenced by relatively high R^2 (i.e. >0.4), but with high bias (i.e. absolute bias >30%) (figures 5(a), (b) and (e), (j)). This may suggest that their training data from spaceborne LiDAR and SAR can capture the 3D features of vegetation leading to model's good sensitivity to AGB density, but the training data were not well calibrated with representative reference data for the model to build realistic relationships between training features and AGB density specifically for NA boreal regions.

Decadal patterns of change diverged among data products (figure S9). In general, most products had a weak to moderate correlation on temporal AGB change. Similar low correlations were also observed among four global AGB datasets (Araza *et al* 2023). As a result, considerable uncertainty remains in estimating AGB decadal change. Yet, time series AGB products are essential to understand how the high-latitude carbon cycle is varying through time, and having uncertain rates of AGB change is an impediment to this goal.

Therefore, we have identified two priority areas for future AGB mapping, which include: (1) to decrease the regional bias in training datasets and resulting AGB maps, and (2) to increase the capability of time-series datasets to capture temporal change of AGB. One direction for addressing these two challenges is to utilize both airborne lidar and field measurements to generate training data that are distributed realistically compared to the AGB distribution in the study domain (e.g. matching distributions in reference data of major plant functional types or disturbance history within the study area). This approach was used by the Liang dataset (Liang *et al* 2025), which contributed to the accuracy of the dataset.

4.4. The value of regional maps and dedicated field campaigns

Advances in computational power and spaceborne LiDAR and SAR technologies have enabled global-scale AGB maps, providing insights into the carbon cycle under climate change and rising disturbances. Our meta-analysis underscores the value of regional and continental AGB maps, which generally offer greater detail and accuracy and lower bias than global products. Beyond supporting accurate carbon accounting and trend monitoring, high quality regional maps can serve as reference data or help optimize algorithms for global AGB mapping (Spawn *et al* 2020, Harris *et al* 2021, Santoro *et al* 2021).

We emphasize the critical role of national institutions and field campaigns in developing high quality carbon data products. For AGB mapping in North American ABRs, the Canadian Forest Service (CFS, Natural Resources Canada) has made major notable contributions: developing national AGB maps (Matasci *et al* 2018, Guindon *et al* 2023), producing diverse forest and disturbance data products (e.g. Hermosilla *et al* 2016), and enabling access to extensive ground plots with high geospatial precision (MAGPlot 2024). CFS and other agencies have also released large airborne LiDAR datasets, enabling high-quality AGB mapping (Liang *et al* 2025). Rigorous accuracy assessments would not be possible without such shared resources. Ensuring that these programs continue to collect and share data is essential to developing credible data products.

NASA's decade-long ABoVE program has been pivotal in developing multiple open-source, state-of-the-art AGB datasets, including: (1) annual 30 m maps spanning 30 years regionally (Wang *et al* 2021) and nearly 40 years continentally (Liang *et al* 2025); (2) a 30 m global boreal forest map for 2020 (Duncanson *et al* 2023); and (3) a 30 m global Arctic–Tundra map for 2020, with time-series products forthcoming (Orndahl *et al* 2025). ABoVE also advanced integration of ground and satellite data through extensive airborne sampling (Miller *et al* 2019), including airborne LiDAR flights (Hoy *et al*, in review) and UAS surveys (Yang *et al* 2025), addressing the scale mismatch in Arctic tundra between plots (<5 m) and satellites (>30 m) (Nelson *et al* 2022, Yang *et al* 2022). The high quality datasets from ABoVE can provide strong foundations for developing next-generation products using NASA's NISAR mission (Kraatz *et al* 2022, Siqueira *et al* 2025).

5. Conclusions

To guide potential user communities in selecting suitable AGB products for North American ABRs, we summarized key information for nine datasets and compared their accuracy, similarity, and sensitivity to disturbances. For North American ABRs, the estimated AGB density varies greatly across jurisdictions and ecoregions; for example, ESA CCI estimates were nearly double those from Duncanson and Xu, leading to large differences in plot-level accuracy. Despite all maps capturing similar relative geographic variability, regional and continental maps generally showed lower bias, and higher spatial or temporal resolution than global products. The annual continental-scale AGB dataset from Liang was appropriate for multiple applications due to its high accuracy and spatiotemporal resolution. This dataset was made possible by extensive ground plots and airborne LiDAR data and the dedicated effort of ABoVE campaigns for North American ABRs. These findings highlight the importance of accessible ground and airborne data, along with region- and domain-specific mapping efforts led by forestry institutions and field campaigns, in producing high-quality regional datasets. Such datasets are essential for accurate carbon accounting and monitoring and serve as valuable inputs for developing robust global-scale products.

Acknowledgment

We acknowledge the NASA ABoVE campaign for the funding under Award 80NSSC23K0140, 80NSSC22K1254 and 80NSSC22K1244, funding from Arizona/NASA Space Grant Consortium award 80NSSC20M0041, funding from NSF Office of Polar Programs—Arctic System Science (OPP-ARCSS) award 2116864, funding from NASA directed to support the Carbon Cycle & Ecosystems Office at Goddard Space Flight Center, and funding from NSF-EnvE (1928048). D Y acknowledges support by the Next-Generation Ecosystem Experiments (NGEE Arctic) project, which is funded by the Office of Biological and Environmental Research in the United States Department of Energy's Office of Science. Any use of trade, firm, or product names is for descriptive purposes only and does not imply endorsement by the U.S. Government. We gratefully acknowledge the

NASA ABoVE community for years of support and countless opportunities for growth and collaboration.

Data availability statement

All data products used in this study are publicly available, and the access to each dataset is summarized in table S1.

Supplementary Information available at https://doi.org/10.1088/1748-9326/ae481a/data1.

Author contributions

Wanwan Liang
Data curation (lead), Formal analysis (equal), Investigation (equal), Methodology (equal), Visualization (equal), Writing – original draft (equal), Writing – review & editing (equal)

Kirsten Bauck 0009-0004-5882-4579
Formal analysis (equal), Investigation (equal), Methodology (equal), Visualization (equal), Writing – original draft (equal), Writing – review & editing (equal)

Devon Maloney 0000-0002-6330-2335
Conceptualization (supporting), Data curation (equal), Formal analysis (equal), Investigation (equal), Methodology (equal), Visualization (equal), Writing – original draft (equal), Writing – review & editing (equal)

Elizabeth Hoy 0000-0002-0104-5118
Conceptualization (lead), Funding acquisition (equal), Methodology (equal), Project administration (equal), Supervision (equal), Writing – original draft (equal), Writing – review & editing (equal)

Paul Montesano 0000-0003-1695-2439
Conceptualization (equal), Funding acquisition (equal), Writing – original draft (equal), Writing – review & editing (equal)

Mark J Lara 0000-0002-4670-7031
Data curation (equal), Writing – review & editing (equal)

Daryl Yang 0000-0003-1705-7823
Data curation (equal), Writing – review & editing (equal)

Jeremy Forsythe 0000-0003-1600-8747
Project administration (equal), Supervision (equal), Writing – original draft (equal), Writing – review & editing (equal)

Laura Duncanson 0000-0003-4031-3493
Data curation (equal), Writing – review & editing (equal)

Xanthe Walker 0000-0002-2448-691X
Supervision (equal)

Jonathan A Wang 0000-0003-2839-0699
Conceptualization (equal), Funding acquisition (equal), Project administration (equal), Supervision (equal), Writing – original draft (equal), Writing – review & editing (equal)

References

Araza A *et al* 2023 Past decade above-ground biomass change comparisons from four multi-temporal global maps *Int. J. Appl. Earth Obs. Geoinf.* **118** 103274

Berner L T *et al* 2024 The Arctic plant aboveground biomass synthesis dataset *Sci. Data* **11** 305

Busby S, Evers C and Holz A 2024 Patterns, drivers, and implications of postfire delayed tree mortality in temperate conifer forests of the western United States *Ecosphere* **15** e4805

Duncanson L *et al* 2023 Aboveground biomass density for high latitude forests from ICESat-2, 2020 (ORNL DAAC) (https://doi.org/10.3334/ORNLDAAC/2186) (Accessed 15 June 2025)

Duncanson L *et al* 2025 Global and Boreal Estimates of Woody Aboveground Biomass for 2020: Filling GEDI's Northern Data Gap with ICESat-2 and Harmonized Landsat Sentinel *Social Science Research Network* (https://doi.org/10.2139/ssrn.5784282)

ESA CCI Biomass 2024 CCI biomass user guide (available at: https://climate.esa.int/en/projects/biomass/) (Accessed 2 July 2025)

Foster A C *et al* 2022 Disturbances in North American boreal forest and Arctic tundra: impacts, interactions, and responses *Environ. Res. Lett.* **17** 113001

Gabarró C *et al* 2023 Improving satellite-based monitoring of the polar regions: identification of research and capacity gaps *Front. Remote Sens.* **4** 952091

Goetz S J, Baccini A, Laporte N T, Johns T, Walker W, Kellndorfer J, Houghton R A and Sun M 2009 Mapping and monitoring carbon stocks with satellite observations: a comparison of methods *Carbon Balance Manage.* **4** 2

Government of Canada 2019 Jurisdiction of Canada (available at: https://open.canada.ca/data/en/dataset/306e5004-534b-4110-9feb-58e3a5c3fd97) (Accessed 2 July 2025)

Guindon L, Villemaire P, Correia D L P, Manka F, Lacarte S and Smiley B 2023 SCANFI: Spatialized CAnadian National Forest Inventory data product (Natural Resources Canada, Canadian Forest Service Laurentian Forestry Centre) 10.23687/18e6a919-53fd-41ce-b4e2-44a9707c52dc (Accessed 15 June 2024)

Harris N L *et al* 2021 Global maps of twenty-first century forest carbon fluxes *Nat. Clim. Change* **11** 234–40

Hermosilla T, Wulder M A, White J C, Coops N C, Hobart G W and Campbell L B 2016 Mass data processing of time series Landsat imagery: pixels to data products for forest monitoring *Int. J. Digit. Earth* **9** 1035–54

Hu K T, Wang J A, Friedl M A, Liang W, Kim J, Zhu X, Morton D C and Randerson J T 2025 ABoVE: Landsat-derived annual dominant land cover in Boreal North America, 1986–2020 (ORNL DAAC) (https://doi.org/10.3334/ORNLDAAC/2423) (Accessed 15 June 2025)

Hu T, Su Y, Xue B, Liu J, Zhao X, Fang J and Guo Q 2016 Mapping global forest aboveground biomass with spaceborne LiDAR, optical imagery, and forest inventory data *Remote Sens.* **8** 565

IPCC 2019 Chapter 2: land–climate interactions *Climate Change and Land: an Ipcc Special Report on Climate Change, Desertification, Land Degradation, Sustainable Land Management, Food Security, and Greenhouse Gas Fluxes in Terrestrial Ecosystems* ed P R Shukla *et al* (Intergovernmental Panel on Climate Change) pp 131–248 (available at: www.ipcc.ch/srccl/chapter/chapter-2/)

Kraatz S, Bourgeau-Chavez L, Battaglia M, Poley A and Siqueira P 2022 Mapping and scaling of *in situ* above ground biomass to regional extent with SAR in the great slave region *Earth Space Sci.* **9** e2022EA002431

Liang W *et al* 2025 ABoVE: Landsat-derived annual aboveground biomass density and uncertainty, 1984–2022 (ORNL DAAC) (https://doi.org/10.3334/ORNLDAAC/2465)

Liu Y Y, Van Dijk A I J M, De Jeu R A M, Canadell J G, McCabe M F, Evans J P and Wang G 2015 Recent reversal in loss of global terrestrial biomass *Nat. Clim. Change* **5** 470–4

MAGPlot 2024 Multi-agency ground plot database (available at: https://open.canada.ca/data/en/dataset/1a73441d-cbe9-485b-bc91-84e07f97193f) (Accessed 2 May 2025)

Matasci G, Hermosilla T, Wulder M A, White J C, Coops N C, Hobart G W, Bolton D K, Tompalski P and Bater C W 2018 Three decades of forest structural dynamics over Canada's forested ecosystems using Landsat time-series and lidar plots *Remote Sens. Environ.* **216** 697–714

Metcalfe D B *et al* 2018 Patchy field sampling biases understanding of climate change impacts across the Arctic *Nat. Ecol. Evol.* **2** 1443–8

Miller C E *et al* 2019 An overview of ABoVE airborne campaign data acquisitions and science opportunities *Environ. Res. Lett.* **14** 080201

National Forest Inventory 2021 Canada's National Forest Inventory –ground-plot data, version 2.0 (available at: https://nfi.nfis.org/en)

Natural Resource Canada 2024 National burned area composite (available at: https://cwfis.cfs.nrcan.gc.ca/datamart) (Accessed 2 July 2024)

Nelson P R *et al* 2022 Remote sensing of tundra ecosystems using high spectral resolution reflectance: opportunities and challenges *J. Geophys. Res.* **127** e2021JG006697

NFI Canada 2024 Multi-agency ground plot database (available at: https://nfi.nfis.org/en/contact) (Accessed 2 May 2025)

Olson D M *et al* 2001 Terrestrial ecoregions of the world: a new map of life on Earth: a new global map of terrestrial ecoregions provides an innovative tool for conserving biodiversity *BioScience* **51** 933–8

Orndahl K M *et al* 2025 Next generation Arctic vegetation maps: aboveground plant biomass and woody dominance mapped at 30 m resolution across the tundra biome *Remote Sens. Environ.* **323** 114717

Pan Y *et al* 2011 A large and persistent carbon sink in the world's forests *Science* **333** 988–93

Rantanen M, Karpechko A Y, Lipponen A, Nordling K, Hyvärinen O, Ruosteenoja K, Vihma T and Laaksonen A 2022 The Arctic has warmed nearly four times faster than the globe since 1979 *Commun. Earth Environ.* **3** 168

Santoro M *et al* 2021 The global forest above-ground biomass pool for 2010 estimated from high-resolution satellite observations *Earth Syst. Sci. Data* **13** 3927–50

Santoro M and Cartus O 2025 ESA biomass climate change initiative (biomass_cci): global datasets of forest above-ground biomass for the years 2007, 2010, 2015, 2016, 2017, 2018, 2019, 2020, 2021 and 2022, v6.0 (NERC EDS Centre for Environmental Data Analysis) (https://doi.org/10.5285/95913ffb6467447ca72c4e9d8cf30501) (Accessed 15 May 2025)

Seedre M, Taylor A R, Brassard B W, Chen H Y H and Jõgiste K 2014 Recovery of ecosystem carbon stocks in young boreal forests: a comparison of harvesting and wildfire disturbance *Ecosystems* **17** 851–63

Seidl R *et al* 2017 Forest disturbances under climate change *Nat. Clim. Change* **7** 395–402

Siqueira P, Bourgeau-Chavez L, Bhogapurapu N, Martinez J, Bilt D, Cook C, French N and Chapman B, 2025. Multitemporal SAR for forest biomass, wetlands and soil moisture over NASA's ABoVE region (available at: https://cce-datasharing.gsfc.nasa.gov/conferences/absbyid/102/45/h/1/) (Accessed 2 July 2025)

Spawn S A and Gibbs H K 2020 Global aboveground and belowground biomass carbon density maps for the year 2010 (ORNL DAAC) (https://doi.org/10.3334/ORNLDAAC/1763) (Accessed 5 June 2024)

Spawn S A, Sullivan C C, Lark T J and Gibbs H K 2020 Harmonized global maps of above and belowground biomass carbon density in the year 2010 *Sci. Data* **7** 112

U.S. Environmental Protection Agency 2010 North America Ecoregion, U.S. EPA Office of Research & Development (ORD) (National Health and Environmental Effects Research Laboratory (NHEERL)) (available at: www.epa.gov/eco-research/ecoregions-north-america) (Accessed 2 February 2025)

UNFCCC 2015 Paris agreement (Article 5) (United Nations Framework Convention on Climate Change) (available at: https://unfccc.int/sites/default/files/english_paris_agreement.pdf) (Accessed 2 May 2025)

Wang J, Farina M K, Baccini A and Friedl M A 2021 ABoVE: annual aboveground biomass for boreal forests of ABoVE core domain, 1984–2014 (ORNL DAAC) (https://doi.org/10.3334/ORNLDAAC/1808) (Accessed 15 June 2024)

Xu L *et al* 2021 Changes in global terrestrial live biomass over the 21st century *Sci. Adv.* **7** eabe9829

Yang D *et al* 2022 Remote sensing from unoccupied aerial systems: opportunities to enhance Arctic plant ecology in a changing climate *J. Ecol.* **110** 2812–35

Yang D *et al* 2025 Ecological Insights from Transferable Plant Biomass Mapping across the Arctic using Highresolution Structure-from-Motion and LiDAR Data *ESS Open Archive* (https://doi.org/10.22541/essoar.175874081.18366907/v1)

Yang H *et al* 2023 Global increase in biomass carbon stock dominated by growth of northern young forests over past decade *Nat. Geosci.* **16** 886–92